An Improved Weak Pressure Gradient Scheme for Single-Column Modeling

JACOB P. EDMAN AND DAVID M. ROMPS

Department of Earth and Planetary Science, University of California, Berkeley, and Earth Sciences Division, Lawrence Berkeley National Laboratory, Berkeley, California

(Manuscript received 15 October 2013, in final form 25 February 2014)

ABSTRACT

A new formulation of the weak pressure gradient approximation (WPG) is introduced for parameterizing large-scale dynamics in limited-domain atmospheric models. This new WPG is developed in the context of the one-dimensional, linearized, damped, shallow-water equations and then extended to Boussinesq and compressible fluids. Unlike previous supradomain-scale parameterizations, this formulation of WPG correctly reproduces both steady-state solutions and first baroclinic gravity waves. In so doing, this scheme eliminates the undesirable gravity wave resonance in previous versions of WPG. In addition, this scheme can be extended to accurately model the emission of gravity waves with arbitrary vertical wavenumber.

1. Introduction

In recent decades, single-column atmospheric models, including cloud-resolving models and single-column versions of global climate models, have come into widespread use as a means to develop and test new parameterizations for use in global climate models. To compare with observations, these limited-domain models are often forced with an observed profile of large-scale ascent (equivalently, a profile of large-scale convergence). This approach, however, has its drawbacks. For example, convergence profiles often contain significant errors, whether they come from observations (Mapes et al. 2003) or reanalysis (Roads et al. 1998). Additionally, forcing the model in this way neglects feedbacks on the large-scale circulation (Randall et al. 1996; Hack and Pedretti 2000) by unrealistically decoupling the large-scale vertical velocity from moist convection (Mapes 1997).

One way to solve these problems is to allow the model to specify its own convergence profile by parameterizing the large-scale dynamics (Sobel and Bretherton 2000), a method dubbed supradomain-scale (SDS) parameterization by Romps (2012b). On the most basic level, an SDS parameterization ingests environmental and modeled profiles of temperature and humidity and uses them to calculate the convergence profile, which is defined by the buoyancy of the column relative to its surroundings. Currently, there are two main paradigms for SDS parameterization, known as the weak temperature gradient approximation (WTG; e.g., Raymond and Zeng 2005) and the weak pressure gradient approximation (WPG; e.g., Romps 2012b). The premise of WTG is that vertical advection of potential temperature relaxes buoyancy differences between the column and the environment on some fixed time scale (Raymond and Zeng 2005; Sessions et al. 2010; Wang and Sobel 2012), while WPG relies on a parameterized form of the pressure gradient force between the column and the environment to determine vertical velocity (Holton 1973; Nilsson and Emanuel 1999; Raymond and Zeng 2000; Kuang 2008; Blossey et al. 2009; Kuang 2011; Romps 2012a,b). Both schemes address the traditional problems listed above, but thus far neither approach has yielded an entirely satisfactory method for SDS parameterization.

Previous work has shown that prior implementations of WPG and WTG are inherently unable to adequately model steady-state and transient behavior in the same simulation; parameter values must be tuned depending on which is of interest (Romps 2012b). However, in numerical simulations, WPG appears to capture the dynamics of the full 3D atmosphere more realistically than WTG (Romps 2012a). In particular, a buoyancy perturbation in a column can trigger ascent both above and below the perturbation; this nonlocal ascent has the potential to trigger moist convection by removing a

Corresponding author address: Jacob P. Edman, Department of Earth and Planetary Science, 449 McCone Hall, University of California, Berkeley, Berkeley, CA 94720.
E-mail: jedman@berkeley.edu

DOI: 10.1175/JAS-D-13-0327.1

convective inhibition layer (Bretherton and Smolarkiewicz 1989; Mapes 1993). Romps (2012a) found that WPG was able to replicate this nonlocal behavior, while WTG can, by definition, only produce ascent at levels with positive buoyancy perturbations.

WPG introduces another difficulty, however. A column coupled to WPG behaves as if it were immersed in a bath of plane waves; for this reason, WPG is sometimes referred to as the damped-wave method (Kuang 2008; Wang et al. 2013). Around the frequency of these plane waves, a buoyancy anomaly in the column can trigger a resonance (with convection in phase with plane-wave-induced ascent) rather than the buoyancy anomaly simply damping away (as would occur by gravity wave emission from the column in two or three dimensions). In general, this resonant behavior is undesirable for a scheme that seeks to parameterize the interaction between a single column's anomalous convection and its anomalous large-scale convergence.

In this paper, we seek to resolve these difficulties by deriving a modified version of WPG in the context of the 1D, linearized, damped, shallow-water equations. We do this for simplicity, but this does not limit the applicability of the results. The shallow-water equations can be thought of as representing an atmosphere that only permits one vertical mode; water layers of different depths approximate different vertical modes. To gain some intuition for this connection, we may think of the shallow-water system as representing the free troposphere: a source of mass in the shallow-water system corresponds to an injection of mass into the free troposphere from the boundary layer, which is associated with latent heating. Thanks to the mathematics relating the shallow-water equations to vertical modes of a stratified fluid, it is straightforward to extend the shallow-water results to the full atmosphere. Section 2 derives analytical solutions to a 1D shallow-water system. This information is then used in section 3 to derive a new and improved set of WPG equations for the shallow-water system. Section 4 calculates—for the benchmark system, WTG, and the old and new WPG—the amplitude of the height anomaly driven by an oscillating source. Those solutions are compared for both inviscid and damped flow in section 5, which demonstrates some advantages of the new WPG scheme over other SDS schemes. Section 6 extends the WPG scheme to a continuously stratified fluid. Section 7 concludes with some discussion.

2. Shallow-water equations

The goal of an SDS scheme is to accurately model the large-scale flow between an atmospheric column and its environment. A good SDS scheme will be able to do two things: 1) remove unforced virtual temperature anomalies from the column on appropriate time scales (i.e., the time scales for gravity waves to exit the column) and 2) generate the correct virtual temperature anomaly in the presence of a steady-state heating anomaly (where the virtual temperature anomaly is made possible by a frictional drag on the flow). Both of these behaviors occur in the one-dimensional, linearized, damped, shallow-water equations. Because we can derive analytical solutions for this system, this is where we begin our analysis.

For a shallow-water system of depth D, source Q ($\mathrm{m\,s^{-1}}$), and Rayleigh-damping time scale $1/\alpha$, the following equations govern a small height perturbation h and a small horizontal velocity u:

$$\partial_t h = -D\partial_x u + Q \quad \text{and} \tag{1}$$

$$\partial_t u = -g\partial_x h - \alpha u. \tag{2}$$

This system relates to the tropical free troposphere (where the Coriolis parameter can be approximated as zero) if we think of mapping h onto the mass of the free troposphere and mapping Q onto the convective mass flux into the free troposphere. Using these equations, we wish to derive two time scales: 1) the transient time scale for unforced height anomalies to exit a column and 2) the steady-state time scale that relates a column's steady-state height perturbation h to the applied steady-state forcing Q.

To begin, we must pick a "column" of the 1D shallow-water system that we will poke (with an initial height anomaly) and prod (with a steady-state mass source). Without any loss of generality, we choose our column as the region from $x = -L_1$ to $x = L_1$. For the transient case, this is all that we need to define. But, for the steady-state case with drag, we can only achieve a steady state if the source in the column is balanced elsewhere by a sink (i.e., there is no net source summed across the entire domain). In the absence of any drag (i.e., $\alpha = 0$), switching on a steady source in the column would generate two shock waves of h anomaly that would travel forever up and down the x axis, and the height anomaly in the column would hold steady. In the presence of drag, however, switching on a steady source in the column would cause the h anomaly in the column to grow ad infinitum as the pressure gradient force tries to push the growing mass anomaly out to larger and larger distances against the countervailing drag force.

For this reason, we define a region of compensating mass sink of size L_2 to either side of the column. As depicted in Fig. 1, the source Q in the column of size $2L_1$ is balanced by an equal and opposite source $-QL_1/L_2$ in the wings of combined size $2L_2$. As shown below, the

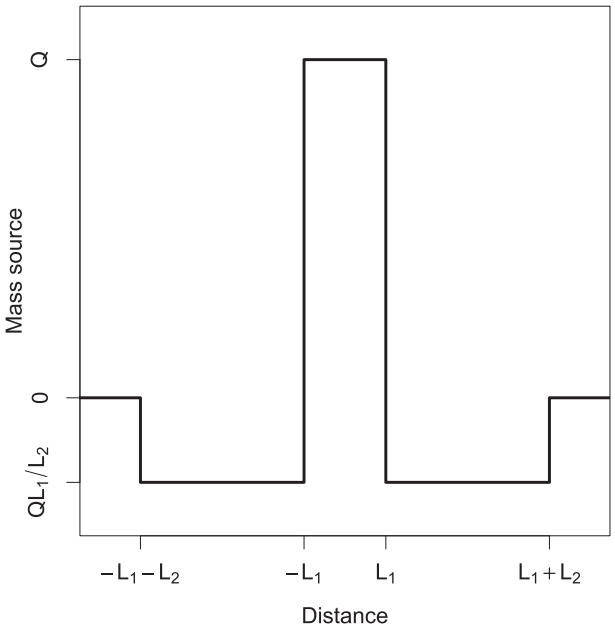

FIG. 1. The setup of the 1D shallow-water forcings. The forcing Q in the column of size $2L_1$ is balanced by an equal and opposite forcing of $-QL_1/L_2$ in the wings of combined size $2L_2$.

choice of L_2 has a negligible impact on the evolution of transients, but it plays a crucial role in defining the magnitude of height anomalies in the presence of a steady-state forcing. What sets L_2? While it is plausible that L_2 may be comparable to the dissipative scale $\sqrt{gD}/\alpha$ (i.e., the product of the wave speed and the damping time scale), we deem it equally plausible that L_2 is set, in reality, by the dissipative effects of the convective response to the passing wave. In this latter scenario, anomalous convection in some column would generate a transient heating of its surroundings by the emitted gravity waves. This transient heating may inhibit convection, leading to an anomalous cooling that damps the wave. If that transient warming is sufficiently efficient at inhibiting convection, then this damping via convective deficit could serve as a sink for the gravity waves well before the waves extend to the dissipative scale. We do not attempt to resolve this difficult issue here. Instead, we simply leave L_2 as a free parameter and leave its determination to future work.

a. Transients

In the study of transients, we will assume that the time scale for inviscid gravity waves to exit the column ($L_1/\sqrt{gD}$) is much smaller than $1/\alpha$, the Rayleigh damping timescale. Therefore, we can safely set $\alpha = 0$. Taking ∂_t of Eq. (1) and $-D\partial_x$ of Eq. (2) and adding the results, we find an inhomogeneous wave equation for h:

$$\partial_t^2 h - gD\partial_x^2 h = \partial_t Q. \tag{3}$$

The solution to Eq. (3) for an arbitrary Q is given by

$$h(x,t) = \frac{1}{2}\int_{-\infty}^{t} dt' \{Q[x + c(t-t'),t'] + Q[x - c(t-t'),t']\}, \tag{4}$$

where $c = \sqrt{gD}$ is the wave speed. Thus, for an initial pulse $Q(x,t) = Q_0(x)\delta(t)$, $h(x,t)$ is given by two waves of the same shape as Q_0, traveling to the left and right with speed c.

Consider a system with zero h for time $t < 0$ that is given an instantaneous jolt at $t = 0$ defined by the source

$$Q(x,t) = \left(1 + \frac{L_1}{L_2}\right) h_0 \delta(t) \mathcal{H}(L_1 - x)\mathcal{H}(L_1 + x) - \frac{L_1}{L_2} h_0 \delta(t)[\mathcal{H}(L_1 + L_2 - x)\mathcal{H}(L_1 + L_2 + x)],$$

where $\mathcal{H}$ is the Heaviside unit step function. This generates $h(x)$ of the same shape as that depicted in Fig. 1, with an initial amplitude in the column of $h = h_0$. The solution, from Eq. (4), is

$$h(x,t) = h_+(x,t) + h_-(x,t),$$

where

$$h_\pm(x,t) = \left(1 + \frac{L_1}{L_2}\right)\frac{h_0}{2}\mathcal{H}(L_1 - x \pm ct)\mathcal{H}(L_1 + x \mp ct) - \frac{L_1}{L_2}\frac{h_0}{2}\mathcal{H}(L_1 + L_2 - x \pm ct)\mathcal{H}(L_1 + L_2 + x \mp ct).$$

This solution is just the sum of top-hat pulses traveling in the negative (h_-) and positive (h_+) directions from the source and sink regions at speed c. The time scale for the entire disturbance to propagate out of the column (defined as $-L_1 < x < L_1$) is on the order of $(L_1 + L_2)/c$. If L_2 is comparable in size to L_1, then this time scale is of order L_1/c. On the other hand, if we assume that the compensating regions are much larger than the width of the column (i.e., $L_2 \gg L_1$), then the amplitude of the disturbance from the compensating regions is small relative to the disturbance from the column. In this case, we can safely ignore this secondary disturbance from the compensating regions, and the time scale for transients to propagate out of the column is still

$$\tau = \frac{L_1}{c} \quad \text{(transient timescale)}. \tag{5}$$

b. Steady state

For the steady-state case, we consider a Q of the same shape as in Fig. 1:

$$Q(x,t) = \left(1 + \frac{L_1}{L_2}\right) Q_0 \mathcal{H}(L_1 - x)\mathcal{H}(L_1 + x) - \frac{L_1}{L_2} Q_0 \mathcal{H}(L_1 + L_2 - x)\mathcal{H}(L_1 + L_2 + x).$$

Assuming a positive α, the steady-state solution to Eqs. (1) and (2) is

$$u(x) = \begin{cases} \dfrac{Q_0}{D} x & |x| \le L_1 \\ \dfrac{Q_0 L_1}{D L_2} \operatorname{sign}(x)(L_1 + L_2 - |x|) & L_1 < |x| < L_1 + L_2 \\ 0 & L_1 + L_2 \le |x| \end{cases} \tag{6}$$

and

$$h(x) = \begin{cases} \dfrac{\alpha Q_0}{2c^2}[L_1(L_1 + L_2) - x^2] & |x| \le L_1 \\ \dfrac{\alpha Q_0 L_1}{2c^2 L_2}(L_1 + L_2 - |x|)^2 & L_1 < |x| < L_1 + L_2 \\ 0 & L_1 + L_2 \le |x| \end{cases}. \tag{7}$$

This solution is shown in Fig. 2. By averaging over the column ($x \in [-L_1, L_1]$), we see that the mean steady-state height anomaly is

$$\frac{1}{2L_1}\int_{-L_1}^{L_1} dx\, h(x) = \frac{\alpha}{c^2} L_1^2 \left(\frac{1}{3} + \frac{1}{2}\frac{L_2}{L_1}\right) Q_0. \tag{8}$$

This equation for the mean height anomaly is of the form τQ_0, where τ is a time scale relating the source Q_0 to the mean steady-state height anomaly in the column. Therefore, we see that this time scale is

$$\tau = \frac{\alpha L_1^2}{c^2}\left(\frac{1}{3} + \frac{1}{2}\frac{L_2}{L_1}\right) \quad \text{(steady-state timescale)}. \tag{9}$$

3. New WPG

WPG reduces Eqs. (1) and (2) to an equation for the evolution of h in a single column embedded in a quiescent environment. The first step in deriving the WPG version of these equations is to take the divergence of Eq. (2). Next, we approximate the resulting pressure gradient term $-\partial_x^2 h$ by h/L^2, where L represents the distance over which the height anomaly (equivalently, the pressure anomaly) relaxes to zero; the precise value

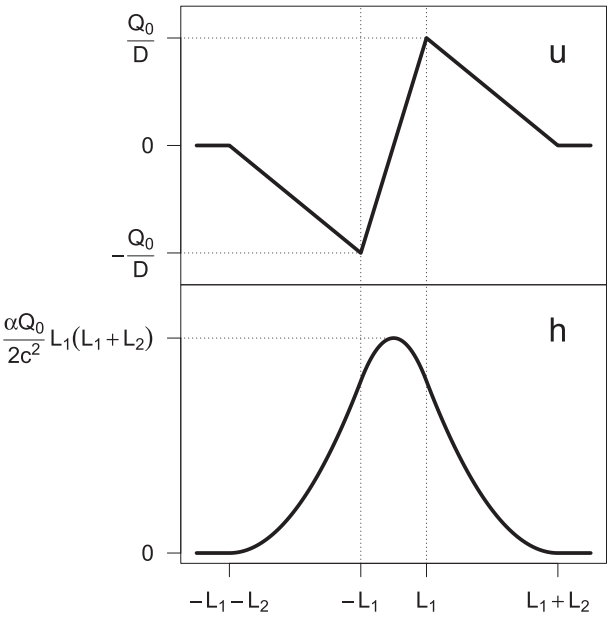

FIG. 2. The steady-state solution corresponding to Eqs. (6) and (7).

of L will be determined below. Finally, we replace α with the to-be-determined constant α^*. This yields the standard WPG equations

$$\partial_t h = -D\delta + Q \quad \text{and} \tag{10}$$

$$\partial_t \delta = \frac{gh}{L^2} - \alpha^* \delta, \tag{11}$$

where $\delta = \partial_x u$ is the divergence. As shown by Romps (2012b), this set of equations is unable to capture simultaneously both the transient and steady-state time scales. Here, we will add a term to the WPG equations in the hope of ameliorating this situation.

The fundamental problem with the WPG equations is that, in the inviscid limit ($\alpha \to 0$), they describe an oscillating system instead of a damped system. If we think of WPG as describing a column immersed in a quiescent environment, then perturbations in the column should exit the column on a gravity wave propagation time scale, causing the perturbation in the column to damp toward zero. Instead, initial perturbations in the WPG system lead to oscillations: in the case of an unforced and inviscid fluid ($Q = \alpha = 0$), Eqs. (10) and (11) give $\partial_t^2 h = -(c/L)^2 h$. This describes a normal mode with period $2\pi L/c$ instead of decay toward zero on a time scale of L/c.

Which of the Eqs. (10) and (11) is responsible for this bad behavior? Equation (10) cannot be at fault because it enforces a simple and irrefutable statement of mass conservation for the column. Equation (11), on the

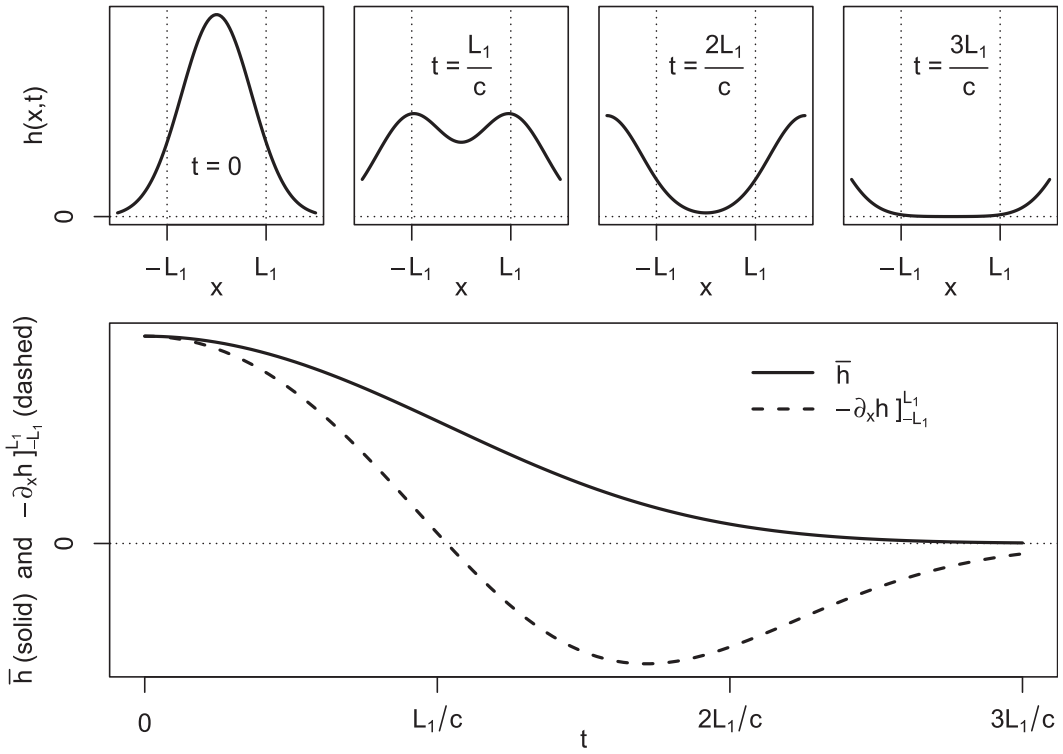

FIG. 3. For a stationary ($\delta = 0$) Gaussian ($h \propto e^{-x^2/L_1^2}$) centered on the column at $t = 0$, the solution for $t > 0$ is of two Gaussians propagating to the left and right. (bottom) The average h in the column ($\overline{h}$, solid curve) decreases monotonically, but the pressure gradient force at the edges of the column ($-\partial_x h|_{-L_1}^{L_1}$, dashed curve) switches from divergent to convergent at $t = 1$. This mismatch between $\overline{h}$ and $-\partial_x h|_{-L_1}^{L_1}$ motivates the addition of a new term to the WPG equations.

other hand, is not as ironclad. Its weak point is the approximation

$$-\overline{\partial_x^2 p} \approx \frac{g}{L^2}\overline{h}, \tag{12}$$

where an overbar denotes an average over $x \in [-L_1, L_1]$. This equation can be written as

$$-\frac{g}{L_1}\partial_x h\Big|_{-L_1}^{L_1} \approx \frac{g}{L^2}\overline{h}.$$

In other words, it assumes that the height gradients at the boundaries of the column are proportional to the mean height perturbation in the column. For a transient height anomaly, however, this is not the case. Consider $\delta = 0$ and $h = h_0 \exp(-x^2/L_1^2)$ at $t = 0$. Taking $Q = \alpha = 0$, this height perturbation evolves as two counterpropagating Gaussian disturbances: one has velocity c, the other has velocity $-c$, and both have an amplitude of $h_0/2$. This is depicted in Fig. 3. For $t < L_1/c$, the mean height anomaly in the column is positive and the pressure gradient force (which is proportional to the height gradient in the shallow-water model) at $x = \pm L_1$ is accelerating fluid out of the column. For $t > L_1/c$, however, the mean height anomaly is still positive, but the pressure gradient force has switched signs and is now accelerating fluid into the column. This example illuminates a key piece of physics missing from the approximation in Eq. (12): the back reaction caused by the column's modification of its immediate environment. Height anomalies initially within the column at time t are just outside the column at time $t + L_1/c$. In this transient case, the difference in height anomalies between the column and its immediate environment is not $\overline{h}(t)$, as assumed in previous implementations of WPG but is, instead, something akin to $\overline{h}(t) - \overline{h}(t - L_1/c) \approx (L_1/c)\partial_t\overline{h}$. This suggests that a term similar to $(L_1/c)\partial_t\overline{h}$ might belong on the right-hand side of Eq. (11).

Note that the h term on the right-hand side of Eq. (11) cannot be entirely replaced by a $\partial_t h$ term because the former is needed to make steady-state solutions possible in the presence of a constant, nonzero Q. Therefore, we explore the consequences of adding the term $(L/c)\partial_t\overline{h}$, multiplied by g/L^2 and a to-be-determined dimensionless number β, to the right-hand side of the divergence equation. This gives

$$\partial_t h = -D\delta + Q \quad \text{and} \tag{13}$$

$$\partial_t \delta = \frac{gh}{L^2} + \frac{\beta g}{Lc}\partial_t h - \alpha^* \delta. \tag{14}$$

To put Eq. (14) in a form more easily integrated, we define a new variable δ' related to δ and h as

$$\delta' = \frac{\delta - \beta g h/cL}{1 - \beta\alpha^* L/c}.$$

Expression (14) benefits from a cancellation of terms when written in terms of δ'. The resulting equations are

$$\partial_t h = -D\delta + Q, \tag{15}$$

$$\partial_t \delta' = \frac{gh}{L^2} - \alpha^* \delta', \quad \text{and} \tag{16}$$

$$\delta = \delta' + \frac{\beta L}{c}\partial_t \delta'. \tag{17}$$

Here, Eq. (16) is a prognostic equation for δ', and Eq. (17) is a diagnostic equation giving δ—the actual divergence—in terms of δ' and its derivative.

To find the correct values for β, L, and α^*, we reduce these equations to a single equation for h and study its steady-state and transient behaviors. The equations reduce to

$$\partial_t^2 h + (\alpha^* + \beta c/L)\partial_t h + \frac{c^2}{L^2} h = \partial_t Q + \alpha^* Q. \tag{18}$$

For transient cases with $Q = 0$, a test solution of $h = e^{\omega t}$ gives a dispersion relation of

$$\omega = -\left(\frac{\alpha^*}{2} + \frac{\beta c}{2L}\right) \pm \sqrt{\left(\frac{\alpha^*}{2} + \frac{\beta c}{2L}\right)^2 - \frac{c^2}{L^2}}. \tag{19}$$

As discussed in section 2a, transients should exit the column on a time scale of L_1/c in the inviscid limit. This is achieved by selecting

$$\beta = 2 \quad \text{and} \tag{20}$$

$$L = L_1, \tag{21}$$

which, in the inviscid limit, reduces Eq. (19) to $\omega = -c/L_1$. For a steady-state case with constant Q, the solution to Eq. (18) is $h = (\alpha^* L^2/c^2)Q$, which yields the time scale found in section 2b if we choose

$$\alpha^* = \alpha\left(\frac{1}{3} + \frac{1}{2}\frac{L_2}{L_1}\right). \tag{22}$$

For the old WPG, $\beta = 0$ in Eq. (18), so there is no way to simultaneously capture the transient time scale and the steady-state time scale. Selecting $L = L_1$, we have two choices for α^* in the old WPG. If we match the transient time scale, then

$$\alpha^* = 2c/L_1.$$

We will call this "version 1" of the old WPG. If we match the steady-state time scale, then we must choose α^* as defined by Eq. (22). We will call this "version 2" of the old WPG.

WTG is similarly unable to capture both the transient and steady-state time scales. In the relaxed form of WTG (e.g., Raymond and Zeng 2005), Eq. (1) is approximated by

$$\delta = \frac{h}{D\tau}, \tag{23}$$

where τ is the time scale over which height differences between the column and the environment are removed. If we match the transient time scale (i.e., the time for a gravity wave to propagate out of the column), then

$$\tau = \frac{L_1}{c}.$$

This is the form of τ most commonly used in the literature (e.g., Raymond and Zeng 2005; Sessions et al. 2010; Wang and Sobel 2011); we will call this "version 1" of WTG. An alternative, but potentially interesting choice, is to match the steady-state time scale, which gives

$$\tau = \frac{\alpha^* L_1^2}{c^2}.$$

We will call this "version 2" of WTG. The equations for all five SDS schemes are listed in Table 1.

TABLE 1. Definitions of the horizontal divergence δ in the five supradomain-scale schemes in the context of the damped shallow-water equations with damping rate α, column of width $2L_1$, and compensating regions of net width $2L_2$. Here, g is the gravitational acceleration, $c = \sqrt{gD}$ is the wave speed, and h is the mean height anomaly in the column.

SDS scheme	Equations for δ
New WPG	$\partial_t \delta' = \frac{gh}{L_1^2} - \alpha\left(\frac{1}{3} + \frac{1}{2}\frac{L_2}{L_1}\right)\delta'$ $\delta = \delta' + \frac{2L_1}{c}\partial_t \delta'$
Old WPG version 1	$\partial_t \delta = \frac{gh}{L_1^2} - \frac{2c}{L_1}\delta$
Old WPG version 2	$\partial_t \delta = \frac{gh}{L_1^2} - \alpha\left(\frac{1}{3} + \frac{1}{2}\frac{L_2}{L_1}\right)\delta$
WTG version 1	$\delta = \frac{gh}{L_1 c}$
WTG version 2	$\delta = \frac{gh}{\alpha L_1^2}\left(\frac{1}{3} + \frac{1}{2}\frac{L_2}{L_1}\right)^{-1}$

4. Solutions to an oscillating source

Although we have shown that WPG can match the full 1D solution for inviscid transient and steady-state cases, so far we have not demonstrated how WPG performs for cases that do not fit neatly into either of these categories. To explore solutions that lie somewhere between inviscid transients and damped steady states, we calculate here solutions to an oscillating mass source. These solutions are compared against each other in section 5.

a. Benchmark

Consider a source of the shape depicted in Fig. 1 that oscillates in time with angular frequency ω:

$$Q(x,t) = \left(1+\frac{L_1}{L_2}\right) Q_0 \cos(\omega t)\mathcal{H}(L_1 - x)\mathcal{H}(L_1 + x) - \frac{L_1}{L_2} Q_0 \cos(\omega t)\mathcal{H}(L_1 + L_2 - x)\mathcal{H}(L_1 + L_2 + x). \tag{24}$$

In the appendix, we derive the solution generated by this forcing for the case of the inviscid (i.e., $\alpha = 0$) shallow-water equations. In this inviscid case, the average height anomaly over the column is $\overline{h}(t) = h_0 \cos(\omega t + \phi)$, where the amplitude h_0 is

$$h_0^{\text{benchmark}} = \frac{Q_0}{\omega}\left[\left(\frac{c}{\omega L_1}\sin\left(\frac{\omega L_1}{c}\right)\left\{\left(1+\frac{L_1}{L_2}\right)\sin\left(\frac{\omega L_1}{c}\right) - \frac{L_1}{L_2}\sin\left[\frac{\omega(L_1+L_2)}{c}\right]\right\}\right)^2 + \left(-1+\frac{c}{\omega L_1}\sin\left(\frac{\omega L_1}{c}\right)\left\{\left(1+\frac{L_1}{L_2}\right)\cos\left(\frac{\omega L_1}{c}\right) - \frac{L_1}{L_2}\cos\left[\frac{\omega(L_1+L_2)}{c}\right]\right\}\right)^2\right]^{1/2}. \tag{25}$$

In the presence of damping ($\alpha > 0$), an analytical solution is not possible, so the damped shallow-water equations are integrated numerically to obtain the value of h_0.

b. New WPG

In the column, Eq. (24) takes the form $Q(t) = Q_0 \cos(\omega t)$. Therefore, to find the corresponding solution from the new WPG scheme, we substitute $Q = Q_0 e^{i\omega t}$, with ω and Q_0 both real, into Eq. (18) with the values of β, L, and α^* given by Eqs. (20)–(22). We then seek a solution of the form $h = h_0 e^{i\omega t + i\phi}$ for real constants h_0 and ϕ. The resulting dispersion relation for ω is

$$-\omega^2 h_0 + (\alpha^* + 2c/L_1)i\omega h_0 + (c^2/L_1^2)h_0 = (i\omega + \alpha^*)Q_0 e^{-i\phi}.$$

For brevity, the α^* notation is retained here, although its value is given by Eq. (22). Solving for h_0, we obtain

$$h_0^{\text{WPG,new}} = \sqrt{\frac{\omega^2 + \alpha^{*2}}{(c^2/L_1^2 - \omega^2)^2 + (\alpha^* + 2c/L_1)^2\omega^2}}\, Q_0. \tag{26}$$

c. Old WPG version 1

The amplitude for version 1 of the old WPG, which is tuned to match the transient time scale, is obtained by setting β to zero in Eq. (18) and setting $L = L_1$ and $\alpha^* = 2c/L_1$, which gives the dispersion relation

$$-\omega^2 h_0 + (2c/L_1)i\omega h_0 + (c^2/L_1^2)h_0 = (i\omega + 2c/L_1)Q_0 e^{-i\phi}.$$

Solving for h_0, we obtain

$$h_0^{\text{WPG,old,v1}} = \frac{\sqrt{\omega^2 + (2c/L_1)^2}}{\omega^2 + (c/L_1)^2} Q_0. \tag{27}$$

d. Old WPG version 2

The amplitude for version 2 of the old WPG, which is tuned to match the steady-state time scale, is obtained by setting β to zero in Eq. (18) and using the same values for L and α^* used by the new WPG. This gives the dispersion relation

$$-\omega^2 h_0 + \alpha^* i\omega h_0 + (c^2/L_1^2)h_0 = (i\omega + \alpha^*)Q_0 e^{-i\phi}.$$

Solving for h_0, we obtain

$$h_0^{\text{WPG,old,v2}} = \sqrt{\frac{\omega^2 + \alpha^{*2}}{(c^2/L_1^2 - \omega^2)^2 + \alpha^{*2}\omega^2}}\, Q_0. \tag{28}$$

e. WTG version 1

For version 1 of WTG, the dispersion relation is

$$i\omega h_0 = -c h_0/L_1 + Q_0 e^{-i\phi},$$

which gives

$$h_0^{\text{WTG,v1}} = \frac{Q_0}{\sqrt{\omega^2 + c^2/L_1^2}}. \tag{29}$$

f. WTG version 2

For version 2 of WTG, the dispersion relation is

$$i\omega h_0 = -\frac{c^2 h_0}{\alpha^* L_1^2} + Q_0 e^{-i\phi},$$

which gives

$$h_0^{\mathrm{WTG,v2}} = \frac{Q_0}{\sqrt{\omega^2 + c^4/(\alpha^{*2} L_1^4)}}. \tag{30}$$

5. Comparison of oscillating solutions

To facilitate a comparison of these amplitudes, let us nondimensionalize the equations with respect to the gravity wave time scale L_1/c. Introducing nondimensional variables denoted by a tilde,

$$\tilde{h}_0 = \frac{c}{L_1 Q_0} h_0,$$

$$\tilde{\omega} = \omega L_1/c,$$

$$\tilde{\alpha} = \alpha L_1/c, \quad \text{and}$$

$$\tilde{\alpha}^* = \alpha^* L_1/c,$$

the amplitudes become

$$\tilde{h}_0^{\mathrm{benchmark}} = \frac{1}{\tilde{\omega}^2}(\{\sin(\tilde{\omega})[(1+r)\sin(\tilde{\omega}) - r\sin(\tilde{\omega}+\tilde{\omega}/r)]\}^2 + \{-\tilde{\omega} + \sin(\tilde{\omega})[(1+r)\cos(\tilde{\omega}) - r\cos(\tilde{\omega}+\tilde{\omega}/r)]\}^2)^{1/2}, \tag{31}$$

$$\tilde{h}_0^{\mathrm{WPG,new}} = \sqrt{\frac{\tilde{\omega}^2 + \tilde{\alpha}^{*2}}{(1-\tilde{\omega}^2)^2 + (\tilde{\alpha}^* + 2)^2\tilde{\omega}^2}}, \tag{32}$$

$$\tilde{h}_0^{\mathrm{WPG,old,v1}} = \frac{\sqrt{\tilde{\omega}^2 + 4}}{\tilde{\omega}^2 + 1}, \tag{33}$$

$$\tilde{h}_0^{\mathrm{WPG,old,v2}} = \sqrt{\frac{\tilde{\omega}^2 + \tilde{\alpha}^{*2}}{(1-\tilde{\omega}^2)^2 + \tilde{\alpha}^{*2}\tilde{\omega}^2}}, \tag{34}$$

$$\tilde{h}_0^{\mathrm{WTG,v1}} = \frac{1}{\sqrt{\tilde{\omega}^2 + 1}}, \quad \text{and} \tag{35}$$

$$\tilde{h}_0^{\mathrm{WTG,v2}} = \frac{1}{\sqrt{\tilde{\omega}^2 + 1/\tilde{\alpha}^{*2}}}, \tag{36}$$

where

$$r \equiv L_1/L_2.$$

Recall that Eq. (31) is for inviscid flow only, while the other equations are for general damping. In section 5c, numerical simulations of the damped shallow-water equations will be used instead of Eq. (31).

a. Inviscid oscillations for large and small $\tilde{\omega}$

For $\tilde{\omega} \gg 1$, the mass added to the column during the positive phase of Q does not propagate significantly out of the column before it is removed by the negative phase of Q. Therefore, the amplitude h_0 is simply equal to $\int_0^{\pi/2} dt Q_0 \cos(\omega t)$, which gives $\tilde{h}_0 = 1/\tilde{\omega}$. The benchmark solution and all of the WPG and WTG schemes give this behavior, which can be confirmed by taking the large-$\tilde{\omega}$ limit of Eqs. (31)–(36).

For $\tilde{\omega} \ll 1$, not all of the SDS parameterizations are equivalent, even in the inviscid case. In the limit of $\tilde{\omega} \to 0$ for inviscid flow, the amplitudes are

$$\tilde{h}_0^{\mathrm{benchmark}} = \left(\frac{1}{3} + \frac{1}{2}\frac{L_2}{L_1}\right)\tilde{\omega}, \tag{37}$$

$$\tilde{h}_0^{\mathrm{WPG,new}} = \tilde{\omega}, \tag{38}$$

$$\tilde{h}_0^{\mathrm{WPG,old,v1}} = 2, \tag{39}$$

$$\tilde{h}_0^{\mathrm{WPG,old,v2}} = \tilde{\omega}, \tag{40}$$

$$\tilde{h}_0^{\mathrm{WTG,v1}} = 1, \quad \text{and} \tag{41}$$

$$\tilde{h}_0^{\mathrm{WTG,v2}} = 0. \tag{42}$$

Note that the benchmark amplitude scales as $\tilde{\omega}$ in the small-$\tilde{\omega}$ limit. This is caused by gravity waves from the adjacent sink regions that propagate into the column. For $\tilde{\omega} = 0$, the solution is simply an inviscid steady state; without any Rayleigh damping, no pressure gradient (i.e., no h gradient) is needed to drive the flow, so $\tilde{h}_0 = 0$. Therefore, the $\tilde{h}_0 \sim \tilde{\omega}$ scaling reflects the approach to an inviscid steady state as $\tilde{\omega}$ is decreased toward zero.

Both the new WPG and version 2 of the old WPG capture the $\tilde{h}_0 \sim \tilde{\omega}$ scaling. An important difference, however, is that these schemes miss the $(1/3 + L_2/2L_1)$ factor in that scaling relationship. In the benchmark simulations, this dependence on L_2 is caused by the fact that a larger sink region (i.e., larger L_2) requires a longer time for the peak of the sink signal to reach the column. This allows the height anomaly in the column to reach a larger amplitude before it is quenched by gravity waves from the sink regions. Since neither the new WPG scheme nor version 2 of the old WPG scheme know anything about L_2 in the absence of damping, it is not possible for them to capture this effect. The other schemes—version 1 of the old WPG and both WTG

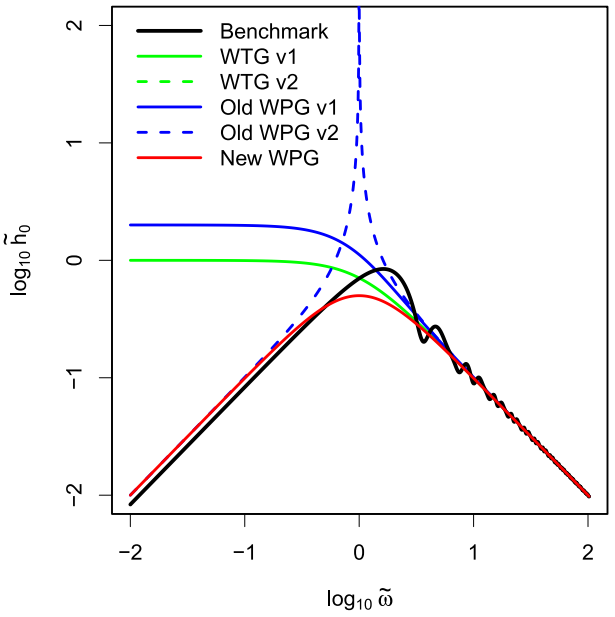

FIG. 4. For inviscid dynamics ($\alpha = 0$) and $L_1/L_2 = 1$, the nondimensionalized amplitude $\tilde{h}_0$ in response to an oscillatory forcing Q with nondimensionalized angular frequency $\tilde{\omega}$.

schemes—are unable to capture any $\tilde{h}_0 \sim \tilde{\omega}$ scaling in the small-frequency limit.

b. *Inviscid oscillations for all $\tilde{\omega}$*

For one-dimensional, inviscid, shallow water, an oscillating source $Q(x, t)$ of the form of Eq. (24) gives rise to height oscillations in the column with an amplitude given by Eq. (31). In the column, this source simplifies to $Q(t) = Q_0 \cos(\omega t)$. When subjected to this $Q(t)$ under the assumption of inviscid flow (i.e., $\alpha = 0$), the five SDS schemes produce height oscillations with amplitudes given by Eqs. (32)–(36) with $\tilde{\alpha}^* = \tilde{\alpha} = 0$.

These amplitudes are plotted as a function of $\tilde{\omega}$ in Fig. 4 for the case of $L_1/L_2 = 1$. The black curve gives the benchmark solution. The green and blue curves correspond to WTG and the old WPG, respectively; solid and dashed curves correspond to version 1 and version 2, respectively. The red curve plots the solution from the new WPG scheme. Note that WTG version 2 (dashed green curve) does not appear on this plot because its h_0 is identically zero when $\tilde{\alpha}^* = 0$. With that exception, all the other schemes do well at matching the benchmark amplitude for large $\tilde{\omega}$. As discussed in the previous section, this agreement at large $\tilde{\omega}$ is a trivial consequence of the forcing period being much smaller than the gravity wave propagation time.

At small $\tilde{\omega}$, the behavior is described by Eqs. (37)–(42). The new WPG scheme and version 2 of the old WPG scheme scale their amplitude in proportion to $\tilde{\omega}$ like the benchmark solution but offset by an overall factor of $1/3 + L_2/2L_1$. The other schemes do poorly in the small-$\tilde{\omega}$ limit.

For $\tilde{\omega} = 1$, versions 2 of WTG and old WPG are both highly discrepant with each other and the benchmark solution: the benchmark has $\tilde{h}_0 \sim 1$, WTG version 2 has $\tilde{h}_0 = 0$, and old WPG version 2 has $\tilde{h}_0 = \infty$. As mentioned above, version 2 of WTG is identically zero for all $\tilde{\omega}$ because it is designed to move height anomalies out of the column on a time scale proportional to α, which is zero in the inviscid limit. Version 2 of the old WPG has a resonance at $\tilde{\omega} = 1$, which manifests itself as an infinite $\tilde{h}_0$ at that frequency. This resonance occurs because that scheme interprets any height anomaly in the column as a consequence of the column sitting in an infinite plane wave of height anomalies with frequency L_1/c. An oscillatory forcing at this frequency is interpreted by this scheme as an amplification of the plane-wave amplitude.

c. *Damped oscillations*

To evaluate the WTG and WPG schemes in the presence of damping ($\alpha > 0$), the benchmark solutions must be simulated numerically. The amplitudes obtained from these numerical simulations are plotted as black circles in Fig. 5, which gives the amplitudes $\tilde{h}_0$ for a range of $\tilde{\omega}$, $\tilde{\alpha}$, and L_1/L_2. The colors and line styles (solid versus dashed) are as in Fig. 4. From left to right, the columns range from $\tilde{\alpha} = 0.1$ to 0.001. From top to bottom, the rows range from $L_1/L_2 = 1$ to 0.01. Each plot depicts $\log_{10}\tilde{h}_0$ as a function of $\log_{10}\tilde{\omega}$, with the abscissa ranging from $\tilde{\omega} = 10^{-4}$ to 10.

The choices of $\tilde{\alpha}$, $\tilde{\omega}$, and L_1/L_2 depicted here are motivated by the following considerations. Imagine that the column (i.e., the region from $-L_1$ to L_1) represents a patch of atmosphere comparable in size to a GCM grid column, that is, with a width on the order of 100 km. For $L_1/L_2 = 1$, any convective anomaly in the column is compensated for by a convective anomaly of comparable magnitude, but opposite sign, in the adjacent grid cells. On the other hand, it is unlikely that the compensating region would be significantly smaller than one grid cell, so we consider $L_1/L_2 = 1$ as the upper limit for this ratio. At the lower limit, we consider $L_1/L_2 = 0.01$, which implies a compensating region on the order of 10 000 km. Since this is already comparable to the circumference of Earth, we take this as the lower limit of L_1/L_2.

A plausible constraint on $\tilde{\omega}$ can be obtained by requiring that gravity waves are able to communicate signals across the compensating region on a short time scale compared to one period of the oscillation; otherwise, the contemporaneous oscillations of the source and sink regions would be acausal. Multiplying the gravity wave speed c by the time scale of the oscillation

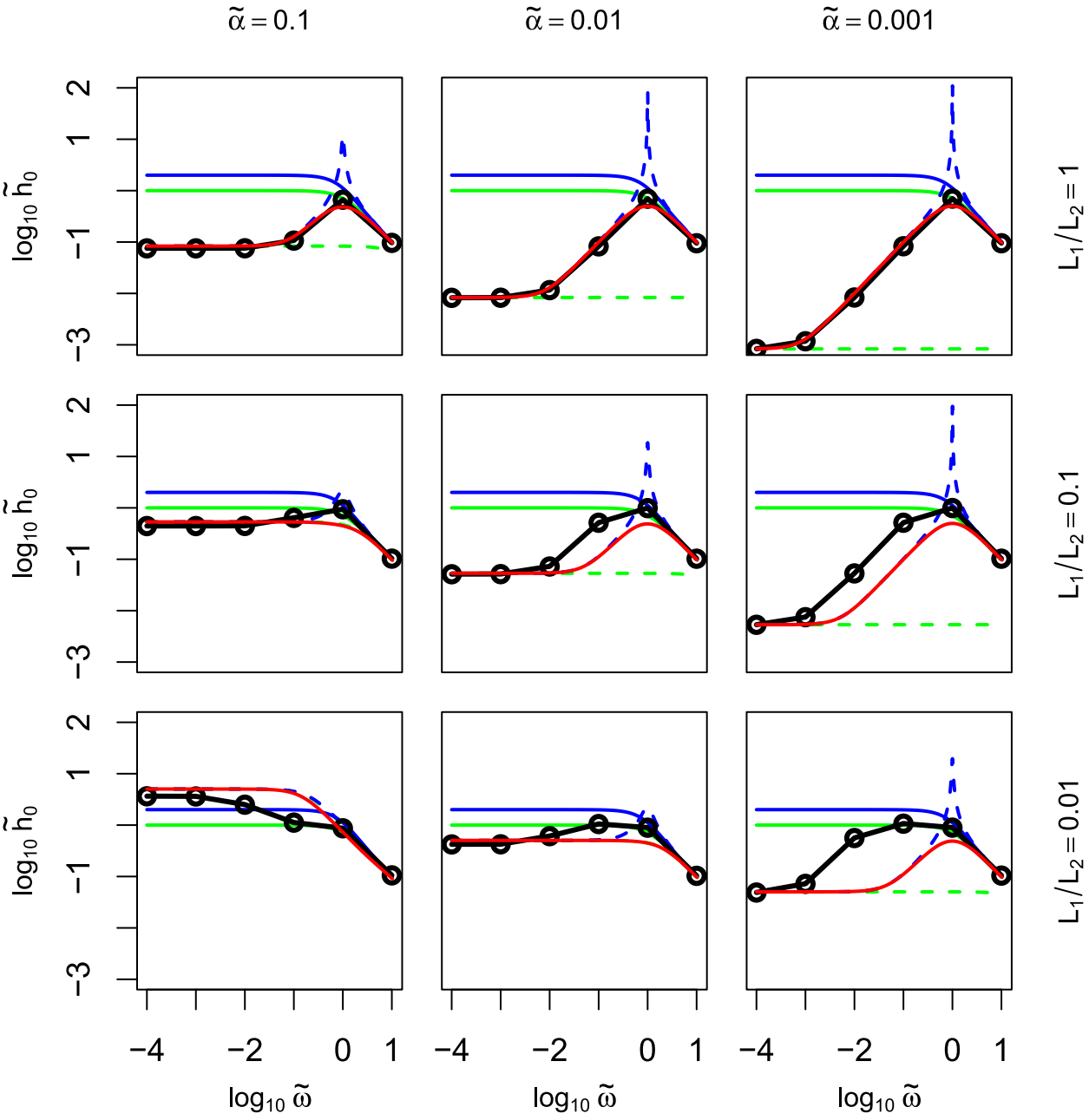

FIG. 5. The nondimensionalized amplitude in response to an oscillatory forcing with nondimensionalized angular frequency. Plots of $\log_{10}(\tilde{h}_0)$ vs $\log_{10}(\tilde{\omega})$ are shown for all combinations of L_1/L_2 = (top) 1, (middle) 0.1, and (bottom) 0.01 and nondimensionalized $\tilde{\alpha}$ = (left) 0.1, (center) 0.01, and (right) 0.001. Results are shown for benchmark numerical model (black circles), WTG version 1 (green solid), WTG version 2 (green dashed), old WPG version 1 (blue solid), old WPG version 2 (blue dashed), and new WPG (red).

$1/\omega$ and requiring it to be larger than L_2, we obtain $c/\omega > L_2$, which can be rewritten as $\tilde{\omega} < L_1/L_2$. In Fig. 5, this region is occupied by $\log_{10}\tilde{\omega} < 0$ in the top row, $\log_{10}\tilde{\omega} < -1$ in the middle row, and $\log_{10}\tilde{\omega} < -2$ in the bottom row. Further consideration of causality leads us to conclude that the maximum size of the sink region L_2 cannot exceed the dissipative scale c/α (i.e., the length scale over which gravity waves are dissipated by Rayleigh damping). This implies that we should restrict our attention to $\tilde{\alpha} \leq L_1/L_2$. For α, a range of $\tilde{\alpha}$ from 0.1 to 0.001 with $c = 50\,\mathrm{m\,s^{-1}}$ and $L_1 = 100\,\mathrm{km}$ corresponds to a range of $1/\alpha$ from 0.2 to 20 days. As shown by Romps (2014), moist convection can generate a damping time scale in the range of 1–10 days, although the precise time

scale depends on the convective mass flux and the baroclinicity of the circulation.

Note that versions 1 of WTG and old WPG give the same curves for $\tilde{h}_0$ in all panels of Fig. 5. This is caused by the fact that the amplitudes in Eqs. (33) and (35) do not depend on either L_2 or α. As in the inviscid case, their amplitudes plateau at small $\tilde{\omega}$, resulting in poor behavior there. Version 2 of WTG is increasingly bad as $\tilde{\alpha}$ decreases, with the amplitude going to zero in the inviscid limit. Version 2 of the old WPG scheme continues to exhibit a resonance at $\tilde{\omega} = 1$, although the addition of damping prevents the amplitude from going to infinity. The new WPG scheme performs very well when L_1 and L_2 are of the same order of magnitude, as shown by the excellent agreement between the black and red curves in the top row of Fig. 5. At smaller L_1/L_2 ratios, the new WPG scheme performs well at small frequencies ($\tilde{\omega} \ll 1$, where the steady state prevails, and so versions 2 of WTG and WPG also perform well) and around one and larger frequencies ($\tilde{\omega} \gtrsim 1$, where transients dominate, and so versions 1 of WTG and WPG also perform well). In these respects, the new WPG combines the best aspects of previous SDS schemes. Where the new WPG is most deficient is for $\tilde{\omega} \sim 0.01$ for the smallest $\tilde{\alpha}$ (0.001) and the smallest L_1/L_2 (0.01). For that combination of $\tilde{\omega}$, $\tilde{\alpha}$, and L_1/L_2, the frequency is large compared to the damping, making the flow practically inviscid. Since L_2 is large compared to L_1, comparison of Eqs. (37) and (38) correctly predicts that the new WPG scheme will underestimate the amplitude by a factor of $L_2/2L_1 = 50$.

6. Extension to continuously stratified fluids

Given an SDS scheme for the shallow-water equations, it is straightforward to extend it to a continuously stratified fluid. Consider the linearized, Rayleigh-damped, hydrostatic, Boussinesq equations described by

$$\partial_t u = -\frac{1}{\rho}\partial_x p - \alpha u, \tag{43}$$

$$\partial_t v = -\frac{1}{\rho}\partial_y p - \alpha v, \tag{44}$$

$$0 = B - \frac{1}{\rho}\partial_z p, \tag{45}$$

$$\partial_t B = -N^2 w + Q, \quad \text{and} \tag{46}$$

$$\partial_x u + \partial_y v + \partial_z w = 0, \tag{47}$$

where B is the buoyancy (m s^{-2}), p is the perturbation pressure (Pa), and Q is the buoyancy source (m s^{-3}). These equations can be combined to give a self-contained equation for B:

$$\partial_t^2\partial_z^2 B + \alpha\partial_t\partial_z^2 B + N^2\nabla^2 B = \partial_t\partial_z^2 Q + \alpha\partial_z^2 Q. \tag{48}$$

For consistency with the one-dimensional shallow-water equations studied in the previous sections, let us drop the y dimension (or, equivalently, consider solutions that are invariant in the y direction). Then, one-dimensional transient waves in an inviscid fluid obey

$$\partial_t^2\partial_z^2 B + N^2\partial_x^2 B = 0.$$

For buoyancy patterns with a vertical wavenumber m, that is, $B(x, z, t) = B(x, t)\sin(mz)$, this is a wave equation with phase speed N/m. Therefore, the transient time scale for these buoyancy patterns is

$$\tau = \frac{L_1 m}{N} \quad \text{(transient timescale)}. \tag{49}$$

Next, consider a steady state, which reduces Eq. (48) to

$$N^2\partial_x^2 B = \alpha\partial_z^2 Q. \tag{50}$$

For a heating of wavenumber m with compensating regions as depicted in Fig. 1, Q takes the form

$$Q(x,z) = \left(1 + \frac{L_1}{L_2}\right) Q_0 \sin(mz)\mathcal{H}(L_1 - x)\mathcal{H}(L_1 + x) - \frac{L_1}{L_2} Q_0 \sin(mz)\mathcal{H}(L_1 + L_2 - x)\mathcal{H}(L_1 + L_2 + x).$$

Substituting this forcing into Eq. (50) along with the test solution $B(x, z) = B(x)\sin(mz)$, we find

$$B(x) = \begin{cases} \dfrac{\alpha Q_0 m^2}{2N^2}[L_1(L_1 + L_2) - x^2] & |x| \le L_1 \\ \dfrac{\alpha Q_0 L_1 m^2}{2N^2 L_2}(L_1 + L_2 - |x|)^2 & L_1 < |x| < L_1 + L_2 \\ 0 & L_1 + L_2 \le |x| \end{cases}. \tag{51}$$

This solution for $B(x)$ is the same as the solution for $h(x)$ in Eq. (7) with c replaced by N/m. In the column, the mean buoyancy anomaly is

$$\frac{1}{2L_1}\int_{-L_1}^{L_1} dx B(x) = \frac{\alpha m^2}{N^2} L_1^2 \left(\frac{1}{3} + \frac{1}{2}\frac{L_2}{L_1}\right) Q_0. \tag{52}$$

Therefore, we see that the time scale relating the forcing Q_0 to the steady-state anomaly is

$$\tau = \frac{\alpha m^2 L_1^2}{N^2}\left(\frac{1}{3} + \frac{1}{2}\frac{L_2}{L_1}\right) \quad \text{(steady-state timescale)}. \tag{53}$$

Not surprisingly, this is the same time scale as in Eq. (9) with c replaced by N/m.

By analogy to the new WPG scheme given in Table 1 for the shallow-water equations, the Boussinesq fluid coupled to the new WPG scheme is described by

$$\partial_t B = -N^2 w + Q, \tag{54}$$

$$\partial_z p = \rho B, \tag{55}$$

$$\partial_z w = -\delta, \tag{56}$$

$$\partial_t \delta' = \frac{1}{\rho}\frac{p}{L_1^2} - \alpha^* \delta', \quad \text{and} \tag{57}$$

$$\delta = \delta' + \frac{2\pi L_1}{HN}\partial_t \delta', \tag{58}$$

with $\alpha^* = \alpha(1/3 + L_2/2L_1)$. Here, B plays a role analogous to that of h in the shallow-water equations. Equations (55) and (56) have no analog in the shallow-water equations but are present here because the Boussinesq system is a continuously stratified fluid. Note that Eqs. (57) and (58) are the same as the new WPG equations listed in Table 1, but with gh replaced by p and c replaced by NH/π, which is the wave speed of the first baroclinic mode. These equations can be combined to give a self-contained equation for B:

$$\partial_t^2 \partial_z^2 B + \alpha^* \partial_t \partial_z^2 B - \frac{2\pi N}{HL_1}\partial_t B - \frac{N^2}{L_1^2} B = \partial_t \partial_z^2 Q + \alpha^* \partial_z^2 Q. \tag{59}$$

For inviscid transients of the form $B(z,t) = B_0 \exp(i\omega t + imz)$, we get

$$m^2\omega^2 - (2\pi N/HL_1)i\omega - (N/L_1)^2 = 0. \tag{60}$$

If $m = \pi/H$, then

$$\omega = \frac{HN}{\pi L_1} i,$$

and B decays with the time scale $L_1\pi/HN$. This is the correct behavior for the first baroclinic mode. In steady state with $Q = Q_0 \sin(mz)$, the WPG equations reduces to

$$B = \frac{\alpha^* m^2 L^2}{N^2} Q_0. \tag{61}$$

For our choice of α^*, this gives the correct relationship between B and Q.

At first glance, one might be concerned by the presence of the dry first baroclinic wave speed in Eq. (58) because moist convection coupled to dry dynamics can generate waves that move at speeds different from the dry gravity wave phase speed. However, this occurs by a superposition of damped, dry, gravity waves, all of which travel at their respective dry phase speeds. To state this in another way, the large-scale gravity wave dynamics are always dictated by a linear set of equations, regardless of the heat source. No matter how nonlinear the interactions between the convective heat source and the gravity waves, the coupled convection–wave dynamics are simply given by the dry, large-scale dynamics coupled to a heat source. The purpose of any supradomain-scale parameterization is to parameterize these large-scale dry dynamics, so the use of the dry gravity wave speed is correct here, and in fact, not unique to WPG. Prior implementations of WTG also use the dry, first baroclinic wave speed to set the relaxation time scale for the temperature profile τ (Raymond and Zeng 2005; Sessions et al. 2010; Wang and Sobel 2011; Daleu et al. 2012).

For a fully compressible atmosphere, such as that simulated by a cloud-resolving model, WPG is implemented by the addition of a mass source $-\rho\delta$ as described by Romps (2012b). In the new WPG scheme, the divergence δ is governed by

$$\partial_t \delta'(z,t) = \frac{\overline{p}(z,t) - p_0(z)}{\overline{\rho}(z,t) L_1^2} - \alpha^* \delta'(z,t) \quad \text{and} \tag{62}$$

$$\delta(z,t) = \delta'(z,t) + \frac{2\pi L_1}{HN}\partial_t \delta'(z,t), \tag{63}$$

with $\alpha^* = \alpha(1/3 + L_2/2L_1)$. This pair of equations replaces Eq. (A1) in the appendix of Romps (2012a). Otherwise, the implementation of this new WPG scheme is identical to that described there and in Romps (2012a).

7. Discussion

This new WPG scheme is motivated by the observation that gravity waves can exert a back reaction on a column of fluid as they exit that column, as illustrated by the change in sign of the dashed curve in Fig. 3. By adding a term to the governing equation for the large-scale divergence, this behavior can be captured. The resulting formulation of WPG can simultaneously capture the time scale of gravity wave transients (i.e., the time it takes for gravity waves to remove transient pressure anomalies from the column) and the time scale for steady-state solutions (i.e., the time that relates the steady-state buoyancy source to the steady-state buoyancy anomaly). As pointed out by Romps (2012b), neither WTG nor the original WPG are able to do this.

One problem that remains, at least superficially, is the inability of this new WPG to simultaneously capture the correct time scales for more than one transient baroclinic mode. In Eq. (58) for WPG in a Boussinesq fluid, the coefficient of the last term contains π/H, which is the vertical wavenumber of the first baroclinic mode. As a consequence, the dispersion relation [Eq. (60)] only gives the correct time scale for transient modes with this wavenumber; higher wavenumbers are damped too quickly. Fortunately, the key to overcoming this problem is straightforward in the new WPG. Following a spectral decomposition approach akin to suggestions by Bergman and Sardeshmukh (2004) and Mapes (2004) and choosing a basis for the baroclinic modes, denoted by $c_k(z)$, we can write p, δ, and δ' as

$$p(z,t) = \sum_k p_k(t)c_k(z), \tag{64}$$

$$\delta(z,t) = \sum_k \delta_k(t)c_k(z), \quad \text{and} \tag{65}$$

$$\delta'(z,t) = \sum_k \delta'_k(t)c_k(z). \tag{66}$$

Equations (57) and (58) can then be modified to

$$\partial_t \delta'_k = \frac{1}{\rho}\frac{p_k}{L_1^2} - \alpha^* \delta'_k \quad \text{and} \tag{67}$$

$$\delta_k = \delta'_k + \frac{2L_1}{N} m_k \partial_t \delta'_k, \tag{68}$$

where $m_k = k\pi/H$. This differs from Eqs. (57) and (58) in that the coefficient in Eq. (68) now contains the vertical wavenumber m_k, which results in a mode-specific phase speed N/m_k. In a practical implementation, this simply requires decomposing p into modes at each time step (truncating at some sufficiently high-wavenumber n) and integrating n prognostic equations for the n different δ'_k. An analogous decomposition can be made for a compressible fluid.

Acknowledgments. This work was supported by the U.S. Department of Energy's Earth System Modeling, an Office of Science, Office of Biological and Environmental Research program under Contract DE-AC02-05CH11231. Thanks are due to Adam Sobel, David Raymond, and an anonymous reviewer for their helpful suggestions that improved this paper.

APPENDIX

Inviscid Shallow-Water Solution with a Top-Hat Oscillating Source

A top-hat mass source that oscillates with angular frequency ω in a column from x_1 to x_2 may be written as

$$Q(x,t;x_1,x_2) = Q_0 \cos(\omega t)\mathcal{H}(x_2 - x)\mathcal{H}(x - x_1).$$

The fundamental solution to the inviscid shallow-water equations from Eq. (4) then becomes

$$h(x,t;x_1,x_2) = \frac{Q_0}{2}\int_{-\infty}^{t} dt' \cos(\omega t')(\mathcal{H}\{x_2 - [x + c(t-t')]\}\mathcal{H}\{[x + c(t-t')] - x_1\} + \mathcal{H}\{x_2 - [x - c(t-t')]\}\mathcal{H}\{[x - c(t-t')] - x_1\}). \tag{A1}$$

We can rewrite the integrand using the identity $\mathcal{H}(ct' - a)\mathcal{H}(b - ct') = \mathcal{H}(ct' - a) - \mathcal{H}(ct' - b)$, which holds provided that $a < b$. In this case, a is always less than b since $x_2 > x_1$. Rewriting Eq. (A1) with this identity, we obtain

$$h(x,t;x_1,x_2) = \frac{Q_0}{2}\int_{-\infty}^{t} dt' \cos(\omega t')\{\mathcal{H}[ct' - (-x_2 + x + ct)] - \mathcal{H}[ct' - (-x_1 + x + ct)] + \mathcal{H}[ct' - (x_1 - x + ct)] - \mathcal{H}[ct' - (x_2 - x + ct)]\}. \tag{A2}$$

This can be broken up into four integrals, with different lower bounds imposed by the step functions:

$$h(x,t;x_1,x_2) = \frac{Q_0}{2}\left\{\int_{t+(x-x_2)/c}^{t} dt' \cos(\omega t')\mathcal{H}[ct' - (ct + x - x_2)] - \int_{t+(x-x_1)/c}^{t} dt' \cos(\omega t')\mathcal{H}[ct' - (ct + x - x_1)] + \int_{t+(x_1-x)/c}^{t} dt' \cos(\omega t')\mathcal{H}[ct' - (ct + x_1 - x)] - \int_{t+(x_2-x)/c}^{t} dt' \cos(\omega t')\mathcal{H}[ct' - (ct + x_2 - x)]\right\}. \tag{A3}$$

Evaluating the integrals leads to the following solution for $h(x, t)$:

$$h(x,t;x_1,x_2)=\frac{Q_0}{2\omega}(\mathcal{H}(x_2-x)\{\sin(\omega t)-\sin[\omega t+\omega(x-x_2)/c]\}-\mathcal{H}(x-x_2)\{\sin(\omega t)-\sin[\omega t+\omega(x_2-x)/c]\}$$
$$-\mathcal{H}(x_1-x)\{\sin(\omega t)-\sin[\omega t+\omega(x-x_1)/c]\}+\mathcal{H}(x-x_1)\{\sin(\omega t)-\sin[\omega t+\omega(x_1-x)/c]\}),\quad \text{(A4)}$$

which can be written as

$$h(x,t;x_1,x_2)=\frac{Q_0}{2\omega}\{\mathrm{sign}(x_2-x)[\sin(\omega t)-\sin(\omega t-\omega|x_2-x|/c)]+\mathrm{sign}(x-x_1)[\sin(\omega t)-\sin(\omega t-\omega|x-x_1|/c)]\}.\quad \text{(A5)}$$

For an oscillating source of the form in Eq. (24), the solution becomes

$$h(x,t)=\left(1+\frac{L_1}{L_2}\right)h(x,t;-L_1,L_1)-\frac{L_1}{L_2}h(x,t;-L_1-L_2,L_1+L_2).\quad \text{(A6)}$$

The average of this function over the column is

$$\overline{h}(t)\equiv\frac{1}{2L_1}\int_{-L_1}^{L_1}dx'h(x',t)\quad \text{(A7)}$$

$$=\frac{Q_0}{\omega}\sin(\omega t)+\frac{Q_0c}{\omega^2 2L_1}\left(1+\frac{L_1}{L_2}\right)\left[\cos(\omega t)-\cos\left(\omega t-\omega\frac{2L_1}{c}\right)\right]\quad \text{(A8)}$$

$$-\frac{Q_0c}{\omega^2 2L_1}\frac{L_1}{L_2}\left[\cos\left(\omega t-\omega\frac{L_2}{c}\right)-\cos\left(\omega t-\omega\frac{2L_1+L_2}{c}\right)\right].\quad \text{(A9)}$$

Written as $\overline{h}(t)=h_0\cos(\omega t+\phi)$, the amplitude h_0 of this oscillation is given by Eq. (25).

REFERENCES

Bergman, J. W., and P. D. Sardeshmukh, 2004: Dynamic stabilization of atmospheric single column models. *J. Climate,* **17,** 1004–1021, doi:10.1175/1520-0442(2004)017<1004:DSOASC>2.0.CO;2.

Blossey, P. N., C. S. Bretherton, and M. C. Wyant, 2009: Subtropical low cloud response to a warmer climate in a superparameterized climate model. Part II: Column modeling with a cloud resolving model. *J. Adv. Model. Earth Syst.,* **1** (3), doi:10.3894/JAMES.2009.1.8.

Bretherton, C. S., and P. K. Smolarkiewicz, 1989: Gravity waves, compensating subsidence and detrainment around cumulus clouds. *J. Atmos. Sci.,* **46,** 740–759, doi:10.1175/1520-0469(1989)046<0740:GWCSAD>2.0.CO;2.

Daleu, C. L., S. J. Woolnough, and R. S. Plant, 2012: Cloud-resolving model simulations with one- and two-way couplings via the weak temperature gradient approximation. *J. Atmos. Sci.,* **69,** 3683–3699, doi:10.1175/JAS-D-12-058.1.

Hack, J. J., and J. A. Pedretti, 2000: Assessment of solution uncertainties in single-column modeling frameworks. *J. Climate,* **13,** 352–365, doi:10.1175/1520-0442(2000)013<0352:AOSUIS>2.0.CO;2.

Holton, J., 1973: A one-dimensional cumulus model including pressure perturbations. *Mon. Wea. Rev.,* **101,** 201–205, doi:10.1175/1520-0493(1973)101<0201:AOCMIP>2.3.CO;2.

Kuang, Z., 2008: Modeling the interaction between cumulus convection and linear gravity waves using a limited-domain cloud system–resolving model. *J. Atmos. Sci.,* **65,** 576–591, doi:10.1175/2007JAS2399.1.

——, 2011: The wavelength dependence of the gross moist stability and the scale selection in the instability of column-integrated moist static energy. *J. Atmos. Sci.,* **68,** 61–74, doi:10.1175/2010JAS3591.1.

Mapes, B., 1993: Gregarious tropical convection. *J. Atmos. Sci.,* **50,** 2026–2037, doi:10.1175/1520-0469(1993)050<2026:GTC>2.0.CO;2.

——, 1997: Equilibrium vs. activation control of large-scale variations of tropical deep convection. *The Physics and Parameterization of Moist Atmospheric Convection,* Springer, 321–356.

——, 2004: Sensitivities of cumulus-ensemble rainfall in a cloud-resolving model with parameterized large-scale dynamics. *J. Atmos. Sci.,* **61,** 2308–2317, doi:10.1175/1520-0469(2004)061<2308:SOCRIA>2.0.CO;2.

——, P. Ciesielski, and R. Johnson, 2003: Sampling errors in rawinsonde-array budgets. *J. Atmos. Sci.,* **60,** 2697–2714, doi:10.1175/1520-0469(2003)060<2697:SEIRB>2.0.CO;2.

Nilsson, J., and K. Emanuel, 1999: Equilibrium atmospheres of a two-column radiative–convective model. *Quart. J. Roy. Meteor. Soc.,* **125,** 2239–2264, doi:10.1002/qj.49712555814.

Randall, D., K. Xu, R. Somerville, and S. Iacobellis, 1996: Single-column models and cloud ensemble models as links between observations and climate models. *J. Climate,* **9,** 1683–1697, doi:10.1175/1520-0442(1996)009<1683:SCMACE>2.0.CO;2.

Raymond, D. J., and X. Zeng, 2000: Instability and large-scale circulations in a two-column model of the tropical troposphere. *Quart. J. Roy. Meteor. Soc.,* **126,** 3117–3135, doi:10.1002/qj.49712657007.

——, and ——, 2005: Modelling tropical atmospheric convection in the context of the weak temperature gradient approximation. *Quart. J. Roy. Meteor. Soc.,* **131,** 1301–1320, doi:10.1256/qj.03.97.

Roads, J., S. Chen, M. Kanamitsu, and H. Juang, 1998: Vertical structure of humidity and temperature budget residuals over

the Mississippi River basin. *J. Geophys. Res.,* **103,** 3741–3759, doi:10.1029/97JD02759.

Romps, D. M., 2012a: Numerical tests of the weak pressure gradient approximation. *J. Atmos. Sci.,* **69,** 2846–2856, doi:10.1175/JAS-D-11-0337.1.

——, 2012b: Weak pressure gradient approximation and its analytical solutions. *J. Atmos. Sci.,* **69,** 2835–2845, doi:10.1175/JAS-D-11-0336.1.

——, 2014: Rayleigh damping in the free troposphere. *J. Atmos. Sci.,* **71,** 553–565, doi:10.1175/JAS-D-13-062.1.

Sessions, S. L., S. Sugaya, D. J. Raymond, and A. H. Sobel, 2010: Multiple equilibria in a cloud-resolving model using the weak temperature gradient approximation. *J. Geophys. Res.,* **115,** D12110, doi:10.1029/2009JD013376.

Sobel, A., and C. Bretherton, 2000: Modeling tropical precipitation in a single column. *J. Climate,* **13,** 4378–4392, doi:10.1175/1520-0442(2000)013<4378:MTPIAS>2.0.CO;2.

Wang, S., and A. H. Sobel, 2011: Response of convection to relative sea surface temperature: Cloud-resolving simulations in two and three dimensions. *J. Geophys. Res.,* **116,** D11119, doi:10.1029/2010JD015347.

——, and ——, 2012: Impact of imposed drying on deep convection in a cloud-resolving model. *J. Geophys. Res.,* **117,** D02112, doi:10.1029/2011JD016847.

——, ——, and Z. Kuang, 2013: Cloud-resolving simulation of TOGA-COARE using parameterized large-scale dynamics. *J. Geophys. Res. Atmos.,* **118,** 6290–6301, doi:10.1002/jgrd.50510.